

# Learning Smooth and Expressive Interatomic Potentials for Physical Property Prediction

Xiang Fu<sup>1</sup>, Brandon M. Wood<sup>1</sup>, Luis Barroso-Luque<sup>1</sup>, Daniel S. Levine<sup>1</sup>, Meng Gao<sup>1</sup>, Misko Dzamba<sup>1</sup>, C. Lawrence Zitnick<sup>1</sup>

<sup>1</sup>Fundamental AI Research (FAIR) at Meta

Machine learning interatomic potentials (MLIPs) have become increasingly effective at approximating quantum mechanical calculations at a fraction of the computational cost. However, lower errors on held out test sets do not always translate to improved results on downstream physical property prediction tasks. In this paper, we propose testing MLIPs on their practical ability to conserve energy during molecular dynamic simulations. If passed, improved correlations are found between test errors and their performance on physical property prediction tasks. We identify choices which may lead to models failing this test, and use these observations to improve upon highly-expressive models. The resulting model, eSEN, provides state-of-the-art results on a range of physical property prediction tasks, including materials stability prediction, thermal conductivity prediction, and phonon calculations.

**Correspondence:** Xiang Fu ([xiangfu@meta.com](mailto:xiangfu@meta.com)) and C. Lawrence Zitnick ([zitnick@meta.com](mailto:zitnick@meta.com))  
**Code:** <https://github.com/FAIR-Chem/fairchem>



## 1 Introduction

Density Functional Theory (DFT), which models the electrons in materials and molecules, serves as the foundation for many modern drug and materials discovery workflows. Unfortunately, DFT calculations are notoriously computationally intensive, scaling cubically with the number of electrons in the system:  $O(n^3)$ . Machine learning interatomic potentials (MLIPs) are promising in approximating and expediting DFT calculations. With increasing data set sizes and model innovations, MLIPs have shown substantial improvements in accuracy and generalization capabilities (Batatia et al., 2023; Merchant et al., 2023; Yang et al., 2024; Barroso-Luque et al., 2024).

Predicting physical properties in chemistry and materials science often requires complex workflows involving numerous evaluations of DFT or MLIPs. For example, in molecular dynamics (MD) simulations, forces are predicted over thousands to millions of time steps. However, the MLIP literature has mostly focused on assessing models based on energy and force predictions over static DFT test sets rather than directly assessing their performance in complex simulations. This approach has limitations, as improved accuracy on test sets does not always lead to better predictions of physical properties (Póta et al., 2024; Loew et al., 2024).

In this paper, we address two questions: Why does higher test accuracy sometimes fail to enhance a model’s ability to predict physical properties, and how can we improve MLIPs to excel in this area? We first outline four critical property prediction tasks and identify the properties required for an MLIP to succeed in these tasks. These properties entail learning a conservative model with continuous and bounded energy derivatives, indicating a smoothly-varying and physically meaningful energy landscape. To test whether these properties hold, we propose testing the ability of MLIPs to practically conserve energy in MD simulations. We demonstrate models that pass this test have a higher correlation between test errors and property prediction accuracy.

Building on these insights, we present a novel MLIP called eSEN and training approach that achieves state-of-the-art (SOTA) performance on complex property prediction tasks. Specifically, our model is capable of running energy-conserving MD simulations for out-of-distribution systems (Figure 1 (a)). For materials stability prediction, eSEN achieves a leading F-1 score of 0.831 and a  $\kappa_{\text{SRME}}$  of 0.321 on the Matbench-Discovery benchmark (Riebesell et al., 2023; Póta et al., 2024). Previous models are only able to excel in one of these metrics (Figure 1 (b,c)). On the MDR Phonon benchmark (Loew et al., 2024), SOTA results are found (Figure 1 (d)).

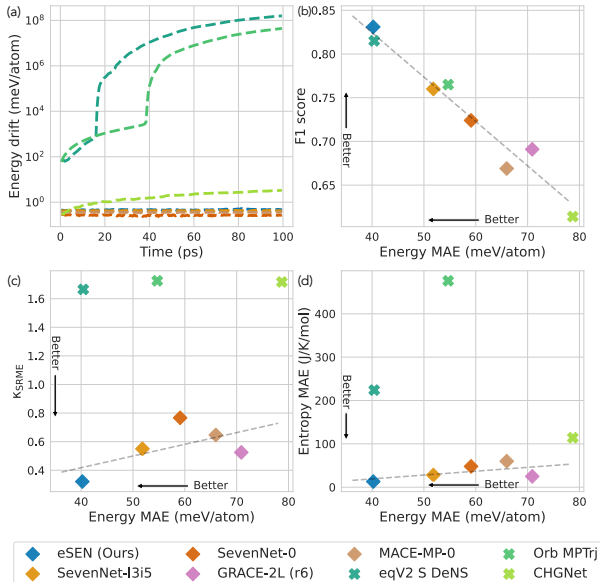


**Figure 1** (a) Energy conservation in MD simulations. Direct-force models (Orb, eqV2) and CHGNet fail to conserve. (b) A higher F-1 score on the Matbench-Discovery strongly correlates with a lower test-set energy MAE. (c) Test-set energy MAE and  $\kappa_{SRME}$  on the Matbench-Discovery benchmark. (d) Test-set energy MAE and vibrational entropy MAE on the MDR Phonon benchmark. Our model (eSEN) achieves the best performance on all benchmarks. A higher correlation between test-set energy MAE and physical property prediction performance can be observed among energy-conserving models. All models are trained on MPTrj.

Finally, eSEN achieves the highest test accuracy on the SPICE-MACE-OFF dataset (Kovács et al., 2023).

## 2 Preliminaries

### 2.1 Machine learning interatomic potentials

Under the Born-Oppenheimer approximation (Oppenheimer, 1927) utilized by DFT (Parr et al., 1979), the Potential Energy Surface (PES) can be written as a function of positions,  $\mathbf{r}$ , and atomic numbers,  $\mathbf{a}$ :  $E(\mathbf{r}, \mathbf{a})$ . Per-atom forces can be calculated by taking the negative gradient of the PES with respect to the atom positions,  $\mathbf{F} = -\nabla_{\mathbf{r}}E$ . For periodic systems such as inorganic materials, the lattice parameters  $\mathbf{l}$  are also considered ( $E(\mathbf{r}, \mathbf{a}, \mathbf{l})$ ), and the stress  $\boldsymbol{\sigma}$  may also be calculated, which can be understood as the gradient of the potential energy surface with respect to the lattice parameters.

The goal of an MLIP (Unke et al., 2021b) is to predict the exact same properties as DFT from a training dataset of DFT calculations (Chanussot et al., 2021;

Riebesell et al., 2023; Loew et al., 2024). The most straightforward benchmark for MLIPs is to evaluate the model on a held-out test set of DFT calculations, and compare models based on the mean absolute error (MAE) or root mean squared error (RMSE) of energies, forces, or stresses. To bridge the gap between these performance metrics and practical applicability, we need to ensure they correlate with physical property prediction tasks, such as those described next.

### 2.2 Physical property prediction tasks

**Geometry optimization/relaxation.** Many computational chemistry and materials science tasks rely on atomic systems being in stable configurations, which correspond to minima of the PES. Stable states are found by minimizing the potential energy using an optimization procedure that iteratively updates atom positions based on the predicted forces ( $\mathbf{F} = -\nabla_{\mathbf{r}}E$ ). Given that many physical properties are evaluated at or near equilibrium states, geometry optimization (also referred to as “relaxation”) is usually the first step in most computational workflows.

**MD simulations.** Simulating the time evolution of atomic systems enables us to gain understanding of various chemical and biological processes, as well as enabling the calculation of macroscopic properties, such as liquid densities, that can be experimentally verified. For the task of molecular dynamics simulation, we typically use a potential to compute the per-atom forces which are then used to numerically integrate Newton’s equations of motion. In this work, we will focus on the **microcanonical ensemble (NVE)**, where the number of particles ( $N$ ), the volume of the system ( $V$ ), and the energy of the system ( $E$ ) are kept constant.

**Phonon and thermal conductivity calculations.** Precise predictions of phonon band structures and vibrational modes are essential for understanding various material properties, including dynamical stability, thermal stability Bartel (2022); Fultz (2010), thermal conductivity Razeghi (2002), and optoelectronic behavior Ganose et al. (2021). The calculation of phonon band structures requires the MLIP to accurately predict higher-order derivatives and capture the subtle curvature of the true PES around critical points. Recent work Póta et al. (2024) has demonstrated the usage of MLIPs in predicting thermal conductivity ( $\kappa$ ) by solving the Wigner transport equation (Simoncelli et al., 2022). In order to accurately predict  $\kappa$ , MLIPs must reliably capture both harmonic and anharmonic phonon behavior, which necessitates the calculation of second and third deriva-

tives of the learned PES.

### 3 Desideratum for physical property prediction

We begin the section by defining what it means for an MLIP to be energy conserving, which is a fundamental principle for applications such as MD simulations (Tuckerman, 2023). For many physical property prediction tasks that probe the higher-order derivatives of the PES it is also important that the PES’s derivatives are well-behaved (they exist and are bounded). To indicate whether a PES meets these criteria, we discuss how an MLIP’s ability to conserve energy given fixed simulation settings may be used.

#### 3.1 Conservative forces

For a force model to be conservative, the work done by moving in a closed path must be zero, i.e., the integration of the forces along any path that starts and ends at the same point is zero:

$$\oint \mathbf{F} \cdot d\mathbf{r} = 0 \quad (1)$$

This property holds if the forces are calculated as the negative derivative of the PES with respect to the atom positions (Unke et al., 2021b). However, predicting forces as derivatives requires an additional backpropagation step through the network, which increases the computational cost of the MLIP. Alternatively, some networks (Liao et al., 2023; Neumann et al., 2024) directly predict forces using a separate force head to increase efficiency<sup>1</sup>. Although direct-force models can achieve high accuracy, their non-conservative nature leads to significantly larger errors in certain property prediction tasks (Fu et al., 2023; Loew et al., 2024; Póta et al., 2024; Bigi et al., 2024).

#### 3.2 Bounded energy derivatives

Conservative forces is a necessary but not sufficient condition for an MLIP to demonstrate energy conservation in MD. In practice, MD simulations use a finite-order numerical integration algorithm and a finite time step  $\Delta t$ , which introduces truncation errors. The most commonly used integrator for the NVE ensemble is the Verlet algorithm—a second-order integrator. The Verlet integrator is known to approximately conserve the total energy of the system in

<sup>1</sup>Strictly speaking, direct-force models are not truly “potentials”, but rather (non-conservative) “force fields”.

long-time simulations. As shown by Theorem 5.1 of Hairer et al. 2003, the total energy drift of a simulation satisfies

$$|E(\mathbf{r}_T, \mathbf{a}) - E(\mathbf{r}_0, \mathbf{a})| \leq C\Delta t^2 + C_N\Delta t^N T, \quad (2)$$

where  $T$ ,  $0 \leq T \leq \Delta t^{-N}$ , is the total simulation time,  $N$  is a positive integer representing the highest order for which the  $N$ th-order derivative of  $E$  is continuously differentiable with a bounded derivative, and  $\mathbf{r}_0$  and  $\mathbf{r}_T$  are the starting and ending positions of the atoms in the simulation respectively. The constants  $C$  and  $C_N$  are independent of  $T$  and  $\Delta t$ . The energy drift bound contains two terms: the first term represents a time-independent fluctuation of  $O(\Delta t^2)$ , and the second term represents the long-term energy conservation. The proof for this theorem is long and technical, for which we refer interested readers to Hairer et al. 2003 and Hairer et al. 2006 for more details.

In Equation (2), the  $\Delta t^N$  in the second term and the bound on the simulation time  $T \leq \Delta t^{-N}$  implies that the PES must be continuously differentiable to high order for energy conservation in long-time simulations. The critical constant  $C_N$  depends on the bounds of the derivatives of  $E$  up to the  $(N + 1)$ th order. This implies that, given a fixed time step size,  $E$  and its higher-order derivatives up to the  $(N)$ th order all need to be continuously differentiable with bounded derivatives to maintain long-time conservation. If the derivatives of a PES are more tightly bound, approximate energy conservation will be maintained even at larger step sizes  $\Delta t$ . Therefore, the magnitude of  $\Delta t$  for which the energy is stable can be viewed as a proxy for the derivative bounds of the estimated PES. Alternatively, if a certain time step is known to be stable when using DFT, we can determine whether an MLIP has similar bounds on higher-order derivatives by testing whether it is also stable using the same time step.

## 4 eSEN

We propose **e**quivariant **S**mooth **E**nergy **N**etwork (**eSEN**), a new MLIP architecture that improves upon architectures that demonstrate high test accuracies to achieve effective physical property predictions. eSEN is a message-passing neural network that conducts multiple blocks of edgewise and nodewise neural processing. Initially, all nodes are embedded as multi-channel spherical harmonic representations. Each eSEN layer block updates the node embedding by conducting an edgewise convolution, followed by a nodewise feed-forward network with normalization layers and residual connections between all layers.

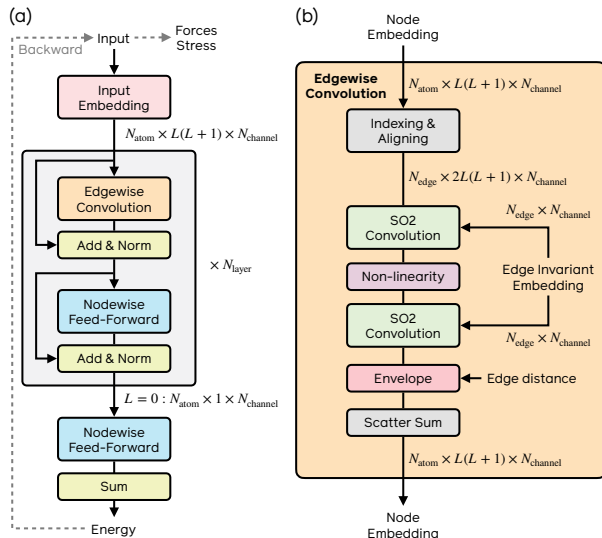


**Figure 2** (a) The eSEN architecture. The high-level architecture is similar to Transformer/Equiformer, while the edgewise/nodewise layers are simplified/enhanced. The final-layer  $L = 0$  features are used to predict nodewise energy, which is summed to get the total potential energy  $E$ . Forces and stress are obtained through back-propagation. (b) The **Edgewise Convolution** layer in eSEN.

A model diagram is shown in Figure 2. eSEN utilizes the same SO2 convolution layer from the equivariant spherical channel network (eSCN) architecture Passaro and Zitnick (2023) inside the edgewise convolution block. Compared to eSCN, our edgewise convolution blocks first concatenate the source and target node embedding, then apply two SO2 convolution layers with an intermediate non-linearity. We also add an envelope function (details in Section 5) which is not in eSCN. The nodewise feed-forward layer uses two equivariant linear layers and an intermediate SiLU-based gated non-linearity (Weiler et al., 2018; Geiger and Smidt, 2022), which is the same as Equiformer (Liao and Smidt, 2022). Unlike eSCN and EquiformerV2 (Liao et al., 2023), which projects the spherical-harmonics channels onto spatial grids for nodewise processing, the nodewise layers in eSEN do not discretize the node representations. As we demonstrate in Section 5, this design improves the ability of the model to conserve energy. Normalization is performed using the equivariant layer normalization (Ba, 2016) proposed by Equiformer (Liao and Smidt, 2022). In the next section, we conduct an in-depth analysis of the key design choices for energy conservation, which we argue is important for accurate physical property prediction.

## 5 Design choices for enhancing physical property prediction

As discussed in Section 3, having conservative forces with continuous and bounded energy derivatives are properties an MLIP should obey for MD simulations. It can also be seen as a prerequisite for the MLIP to accurately capture higher-order behavior of the PES and thus high accuracy in physical property prediction tasks such as phonon calculations. Motivated by this observation, we identify design choices that impact a model’s ability to conserve energy and whether its PES varies smoothly. These design choices can be categorized into three aspects: (1) conservative vs. direct-force prediction; (2) discretization of the representation; and (3) obtaining a continuous and smoothly varying PES. For many of these design aspects, their impact on the desired properties is not well understood.

To quantify whether an MLIP’s PES is continuous and smoothly varying, we measure the ability of the resulting MLIP to conserve energy during MD simulations with a predetermined fixed time step. We trained eSEN models under the same hyperparameters while ablating one design choice at a time. We construct out-of-distribution (OOD) MD simulation tasks for both inorganic materials and organic molecules using models trained on the MPTrj (Jain et al., 2013; Deng et al., 2023) and the SPICE-MACE-OFF (Eastman et al., 2023; Kovács et al., 2023) datasets. For inorganic materials, we compute an average conservation error over 81 NVE MD simulations of 100 ps based on the TM23 dataset’s simulation settings (Owen et al., 2024). For organic molecules, we compute an average conservation error over 7 NVE MD simulations of 100 ps based on the MD22 dataset’s simulation settings (Chmiela et al., 2023). All eSEN models are 2-layer with 3.2M trainable parameters. We include details regarding the task protocol in Appendix A.

### 5.1 Direct-force prediction

Models that directly predict forces  $\hat{\mathbf{F}}$  from the atomic configuration may produce forces that are inconsistent with the energy prediction, i.e.,  $\hat{\mathbf{F}} \neq -\nabla_r \hat{E}$ , and more importantly are unlikely to be conservative. From the perspective of minimizing the test error, the direct-force approach has strong motivations: it avoids the backward pass for force prediction, which significantly improves model efficiency and enables low-precision training which further accelerates training. Empirically, current SOTA accuracy on the

OC20, OC22, and Matbench-Discovery (Chanussot et al., 2021; Tran et al., 2023; Riebesell et al., 2023) benchmarks are achieved by direct-force models. Despite this, the direct-force formulation results in significant energy drift in MD simulations, as shown in Figure 4 (a1, a2). For this reason, we compute forces as the negative gradient of the PES with respect to the atom positions in eSEN.

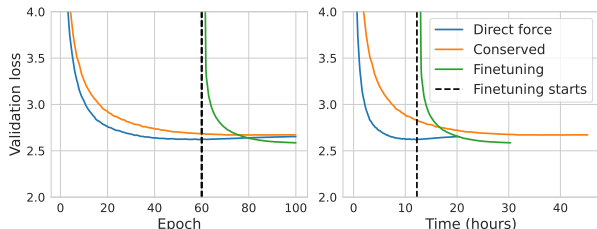


**Figure 3** Validation loss curves for epoch and wallclock time.

**Direct-force pre-training.** Although direct-force models are not suitable for certain physical property prediction tasks, they may still offer advantages (Bigi et al., 2024; Amin et al., 2025). We demonstrate their efficiency can offer significant benefit as a pre-training strategy for a conservative model. Figure 3 shows the validation loss of 2-layer eSEN models trained on the MPTrj dataset: direct-force, conservative, and conservative fine-tuning from a pre-trained direct-force backbone. For conservative fine-tuning, we start from a direct-force model trained for 60 epochs, remove its direct-force prediction head, and fine-tune using conservative force prediction. The conservative fine-tuned model achieves a lower validation loss after being trained for 40 epochs compared to the from-scratch conservative model being trained for 100 epochs. The fine-tuning strategy also reduces the wallclock time for model training by 40%.

## 5.2 Representation discretization

As proposed by Cohen and Welling 2016 and later used in eSCN and EquiformerV2 (Zitnick et al., 2022; Passaro and Zitnick, 2023; Liao et al., 2023), non-linearities may be performed by projecting the spherical harmonics to a discrete grid. A  $1 \times 1$  convolution or pointwise non-linearity may then be applied to this grid, which then get projected back to the spherical-harmonics space. The non-linear step may introduce higher-frequency signals than cannot be properly represented by the spherical harmonics, i.e., they are beyond the Nyquist frequency. This can lead to sampling errors that break strict equivariance and energy conservation. This problem can be mitigated by sampling the grid at higher resolutions as shown

in Figure 4 (b1, b2). In eSEN, we instead use the SiLU-based equivariant Gated non-linearity (Weiler et al., 2018; Geiger and Smidt, 2022) that performs the non-linearity directly in the spherical harmonic representation. This does not require a projection to a discrete grid, so the model is perfectly equivariant and conservative up to numerical accuracy.

## 5.3 Smoothly varying PES

Subtle choices in the design of MLIPs can have a significant impact on whether a PES varies smoothly and can even lead to the presence of discontinuities. These include how neighboring atoms are chosen, whether envelope functions are used near atom distance cutoffs, and which basis functions are used to embed pairwise atom distances. We discuss each of these in turn.

**A maximum number of neighbors limit** in graph construction has been found to improve training efficiency without compromising test error (Liao et al., 2023; Qu and Krishnapriyan, 2024). However, it results in a discontinuity in the learned PES as the nearest-K neighbors may change drastically under a small perturbation of the atom positions. As shown in Figure 4 (c1, c2), having a maximum neighbor limit breaks energy conservation. In eSEN, instead of limiting the number of neighbors, we use the common approach of applying a distance cutoff ( $6\text{\AA}$ ) under which all neighbors are kept.

**Envelope functions** were first introduced in the DimeNet architecture (Gasteiger et al., 2020a) to improve model smoothness. The radial basis function used in MLIPs is not twice continuously differentiable due to the use of a finite cutoff during graph construction. By applying a polynomial envelope function on the edge messages, the values in an edge message and its first/higher-order derivatives with respect to atom positions decays to 0 when the edge distance approaches the cutoff distance. Figure 4 (c1, c2) shows a model fails to conserve energy without the envelope function.

**Radial basis functions** are commonly used to embed interatomic distances (Bartók et al., 2013). A larger number of basis functions (512 in Passaro and Zitnick 2023, as opposed to 10 in eSEN’s default setting) allows higher-frequency signals to pass through the network. This can lead to the PES being more sensitive to small shifts in the atom positions. In our experiments, using a large number of basis functions breaks conservation for the TM23 tasks, but is able to conserve energy for the MD22 tasks. Using a Bessel radial basis function (as opposed to a Gaussian ra-

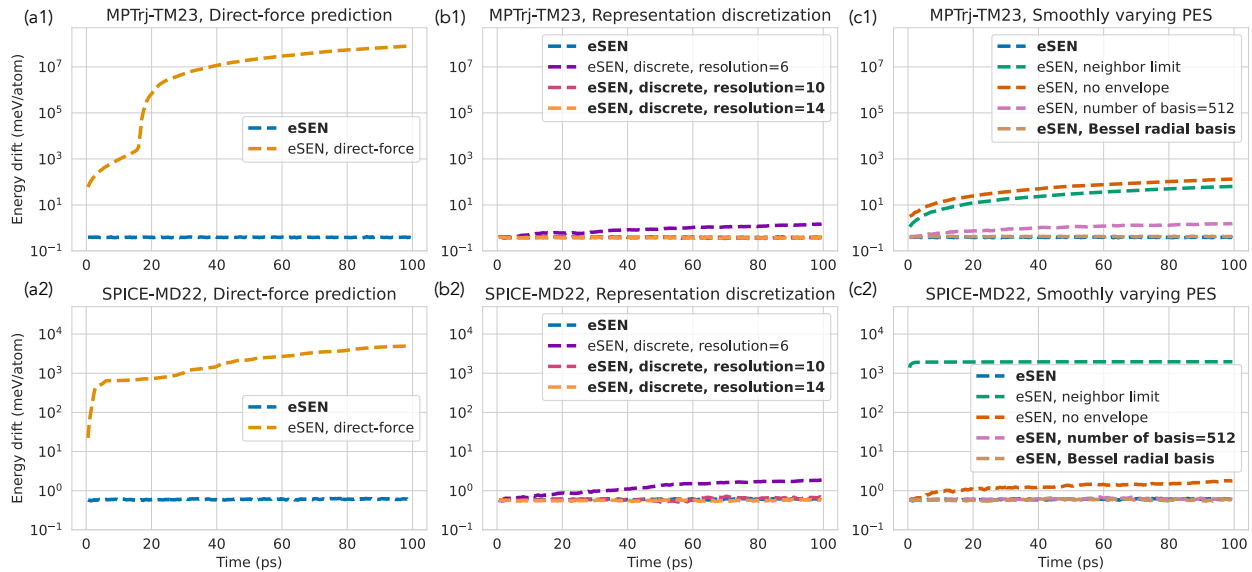


**Figure 4** Conservation error on the TM23 task (top row) and MD22 task (bottom row) for ablating design choices of eSEN. Models that conserve energy are **bolded** in the legends.

**Table 1** Test set MAE for design choices studied in Section 3. The conserved model significantly outperforms the direct-force model on SPICE-MACE-OFF.  $N_{\text{basis}} = 512$  performs slightly better on SPICE but slightly worse on MPTrj. Other eSEN variants all have similar test errors on MPTrj/SPICE-MACE-OFF. Energy MAE is in meV/atom. Force MAE is in meV/Å. Stress MAE is in meV/Å/atom.

Model	MPTrj			SPICE	
	Energy	Force	Stress	Energy	Force
eSEN	17.02	43.96	0.14	0.23	6.36
eSEN, direct	18.66	43.62	0.16	0.56	10.98
eSEN, neighbor limit	17.30	44.11	0.14	0.24	6.52
eSEN, no envelope	17.60	44.69	0.14	0.23	6.33
eSEN, $N_{\text{basis}} = 512$	19.87	48.29	0.15	0.19	5.40
eSEN, Bessel	17.65	44.83	0.15	0.20	5.54
eSEN, discrete, res=6	17.05	43.10	0.14	0.26	6.34
eSEN, discrete, res=10	17.11	43.13	0.14	0.33	6.57
eSEN, discrete, res=14	17.12	43.09	0.14	0.33	6.51

dial basis in the default setting) does not impact conservation properties in both tasks.

## 5.4 Ablation studies

Many of the architecture choices described above have negligible impact on the test set errors as shown in Table 1. However, as shown in Figure 4, they can have a dramatic impact on whether a model is conservative in practice. If a model is found to be conservative, stronger correlations are found between test errors and property prediction tasks (Figure 1 and Figure 6).

## 6 Experiments

In the previous section, we demonstrated the design of eSEN results in its ability to be energy-conserving in MD simulations. In this section, we evaluate eSEN in physical property prediction tasks: (1) materials stability prediction based on geometry optimization; (2) thermal conductivity prediction; and (3) phonon calculation. We also demonstrate the correlation between test energy MAE and physical property prediction tasks for eSEN.

### 6.1 Matbench Discovery

**The Matbench-Discovery benchmark** evaluates a model’s ability to predict ground-state (0 K) thermodynamic stability through geometry optimization and energy prediction. It is a widely used benchmark for evaluating ML models in materials discovery. The compliant benchmark only includes models trained on the MPTrj (Jain et al., 2013; Deng et al., 2023) dataset or its subset, which facilitate a fair comparison of model architectures. The F1 score is the primary metric used to rank models. We train an eSEN with 30M parameters on MPTrj for 60 epochs of direct-force pre-training and 40 epochs of conservative fine-tuning. DeNS (Liao et al., 2024) is used during direct-force pre-training. As shown in Table 2, eSEN-30M achieves an F1 score of 0.831—the highest among all compliant models.

**The thermal conductivity prediction task** requires accurate modeling of harmonic and anharmonic phonons

**Table 2** Matbench-Discovery benchmark results of compliant models (trained only on MPTrj or its subset) with results on the unique prototype split. MAE is in units of eV/atom. ( $\uparrow$ ) stands for higher the better. ( $\downarrow$ ) stands for lower the better.

Model	eSEN-30M	eqV2 S DeNS	Orb MPTrj	SevenNet-l3i5	SevenNet-0	GRACE-2L (r6)	MACE-MP-0	CHGNet	M3GNet
F1 $\uparrow$	<b>0.831</b>	0.815	0.765	0.760	0.724	0.691	0.669	0.613	0.569
DAF $\uparrow$	<b>5.260</b>	5.042	4.702	4.629	4.252	4.163	3.777	3.361	2.882
Precision $\uparrow$	<b>0.804</b>	0.771	0.719	0.708	0.650	0.636	0.577	0.514	0.441
Recall $\uparrow$	0.861	<b>0.864</b>	0.817	0.821	0.818	0.757	0.796	0.758	0.803
Accuracy $\uparrow$	<b>0.946</b>	0.941	0.922	0.920	0.904	0.896	0.878	0.851	0.813
MAE $\downarrow$	<b>0.033</b>	0.036	0.045	0.044	0.048	0.052	0.057	0.063	0.075
R2 $\uparrow$	<b>0.822</b>	0.788	0.756	0.776	0.750	0.741	0.697	0.689	0.585
$\kappa_{\text{SRME}} \downarrow$	<b>0.321</b>	1.665	1.725	0.550	0.767	0.525	0.647	1.717	1.412

in materials, which tests the accuracy of second and third order derivatives of the learned PES. The primary metric is the symmetric relative mean error in predicting thermal conductivity ( $\kappa_{\text{SRME}}$ ). We follow the protocol set forth in the Matbench-Discovery benchmark Riebesell et al. (2023); Póta et al. (2024) to predict thermal conductivity  $\kappa$ . After running a structural relaxation,  $\kappa$  is computed using second and third order force constants obtained from phonon calculations using the supercell method.

As shown in Table 2, our model achieves a  $\kappa_{\text{SRME}}$  of 0.321 under the default evaluation protocol proposed by Póta et al. 2024. Notably, our model excels in both the F1 score and  $\kappa_{\text{SRME}}$ , while all previous models only achieve SOTA performance on one or the other of these metrics.

## 6.2 MDR phonon benchmark

The MDR Phonon benchmark (Loew et al., 2024) assesses the performance of MLIPs in predicting key phonon properties, including maximum phonon frequency ( $\omega_{\text{max}}$ ), entropy ( $S$ ), free energy ( $F$ ) and heat capacity at constant volume ( $C_V$ ). The evaluation follows the testing protocol outlined by Loew et al. 2024. Section 6.2 shows the resulting MAE of our model and those of several other models<sup>2</sup>. eSEN achieves SOTA results, demonstrating a significant improvement over SevenNet, the second most accurate model.

Our results are consistent with those reported by Loew et al. 2024, showing that conservative MLIPs significantly outperform direct-force models in terms of prediction accuracy when tested using phonon calculations with a displacement of 0.01 Å. The high error of direct-force models can be largely attributed

<sup>2</sup>In addition to our model, we also run the evaluation for GRACE-2L (r6) (Bochkarev et al., 2024), SevenNet-l3i5 (Park et al., 2024), Orb MPTrj (Neumann et al., 2024), and eqV2 S DeNS (Liao et al., 2023; Barroso-Luque et al., 2024), which were not included in the work by Loew et al. 2024.

**Table 3** Summary of the MAE for the MPTrj-trained models on the MDR Phonon benchmark. Metrics include maximum phonon frequency ( $\text{MAE}(\omega_{\text{max}})$ , in K), the vibrational entropy ( $\text{MAE}(S)$ , in J/K/mol), the Helmholtz free energy ( $\text{MAE}(F)$ , in kJ/mol), and the heat capacity at constant volume ( $\text{MAE}(C_V)$ , in J/K/mol).

Model	$\text{MAE}(\omega_{\text{max}})$	$\text{MAE}(S)$	$\text{MAE}(F)$	$\text{MAE}(C_V)$
M3GNet	98	150	56	22
CHGNet	89	114	45	21
MACE	61	60	24	13
GRACE-2L (r6)	40	25	9	5
SevenNet-0	40	48	19	9
SevenNet-l3i5	26	28	10	5
eSEN-30M	<b>21</b>	<b>13</b>	<b>5</b>	<b>4</b>
<i>Direct-force models</i>				
Orb MPTrj [0.01 Å]	309	476	64	181
Orb MPTrj [0.2 Å]	61	34	11	8
eqV2 S DeNS [0.01 Å]	280	224	54	94
eqV2 S DeNS [0.2 Å]	58	26	8	8

to high-frequency prediction errors at small displacements Loew et al. (2024). Increasing the displacement used in the finite-difference phonon calculations to 0.2 Å can considerably improve prediction accuracy of direct-force models (with caveats). We include a more detailed analysis of the relationship between atom displacement and phonon prediction in Appendix B.

In physical phonon calculations, we expect the results to converge as the displacement goes to zero. By examining the resulting phonon band structure, we can gain insight into this behavior. Figure 5 presents the predicted phonon band structure and density of states for three representative materials using eSEN. The predicted phonon bands exhibit convergence as the displacement decreases. In contrast, Figures Figure C.11 and Figure C.12 display the phonon bands for the same three materials predicted using eqV2 S DeNS (direct-forces), which not only fail to demonstrate convergence but also exhibit significant errors, including missing acoustic branches and spurious imaginary frequencies.

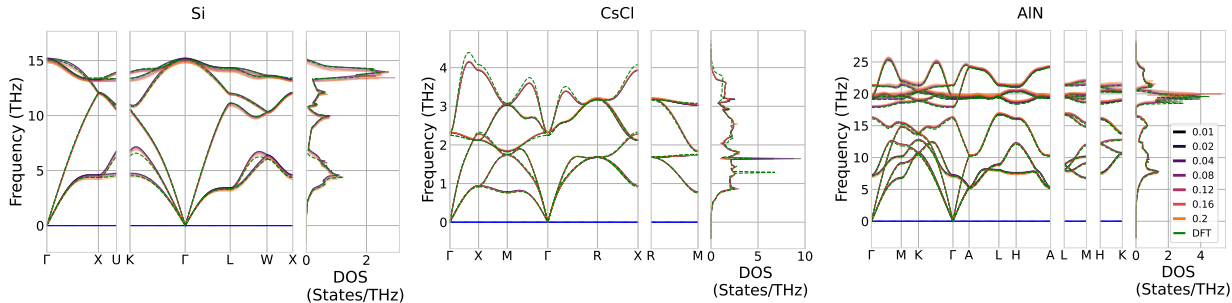


**Figure 5** Predicted phonon band structure and density of states (DOS) of Si (diamond structure), CsCl (CsCl structure), AlN (wurtzite structure) using eSEN at different displacement values. DFT baseline is taken from the PBE MDR dataset [Loew et al. \(2024\)](#) calculated using a displacement of 0.01 Å.

**Table 4** Test set MAE for SPICE-MACE-OFF. Energy (**E**) MAE is in meV/atom. Force (**F**) MAE is in meV/Å. \*EscAIP-45M is a direct-force model.

Dataset	MACE-4.7M		EScAIP-45M*		eSEN-3.2M		eSEN-6.5M	
	E	F	E	F	E	F	E	F
PubChem	0.88	14.75	0.53	5.86	0.22	6.10	<b>0.15</b>	<b>4.21</b>
DES370K M.	0.59	6.58	0.41	3.48	0.17	1.85	<b>0.13</b>	<b>1.24</b>
DES370K D.	0.54	6.62	0.38	2.18	0.20	2.77	<b>0.15</b>	<b>2.12</b>
Dipeptides	0.42	10.19	0.31	5.21	0.10	3.04	<b>0.07</b>	<b>2.00</b>
Sol. AA	0.98	19.43	0.61	11.52	0.30	5.76	<b>0.25</b>	<b>3.68</b>
Water	0.83	13.57	0.72	10.31	0.24	3.88	<b>0.15</b>	<b>2.50</b>
QMugs	0.45	16.93	0.41	8.74	0.16	5.70	<b>0.12</b>	<b>3.78</b>

### 6.3 SPICE-MACE-OFF

We train and evaluate eSEN models on the SPICE-MACE-OFF dataset ([Kovács et al., 2023](#)), which is built upon the SPICE dataset ([Eastman et al., 2023](#)). As shown in [Table 4](#), eSEN with 6.5M parameters outperforms MACE-OFF-L (4.7M parameters) and EscAIP (45M parameters, direct-force) on all test-set splits for both energy and force MAE. We also include results for eSEN with 3.2M parameters, which has inference efficiency similar to MACE-4.7M, while achieving lower test energy/force MAE. More details on the inference efficiency benchmark are included in [Appendix C](#).

### 6.4 Test-set error for model development

In [Figure 1](#), we showed the correlation between test error and physical property prediction tasks for different architectures. [Figure 6](#) demonstrates this correlation for different variants of eSEN (with a 1k-materials subset of the MDR Phonon benchmark for efficiency). In particular, among models that pass the MD energy conservation test, a strong correlation between test error and  $\kappa_{\text{SRME}}$ /vibrational entropy MAE can be observed. We include experimental details about [Figure 1](#) and [Figure 6](#) in [Appendix A](#) and additional results for other phonon properties in [Appendix B](#).

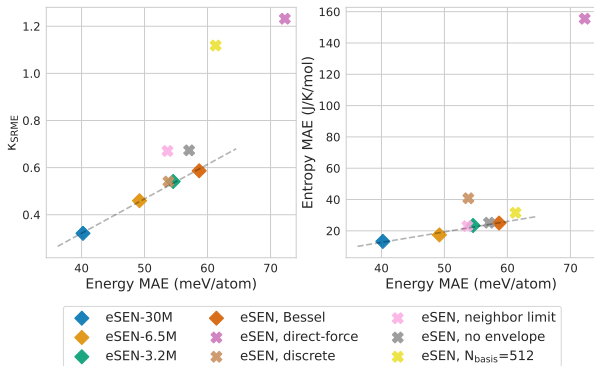


**Figure 6** Test error correlation across several property prediction tasks for eSEN variants. Conservative models are shown as boxes and those found to not conserve are shown as crosses. Note metrics for conservative models have a stronger correlation with test set errors.

## 7 Related works

**MLIP architectures** have made significant progress since their initial proposal ([Behler and Parrinello, 2007](#)). These architectures are usually symmetry-preserving ([Smith et al., 2017](#); [Schütt et al., 2017](#); [Gilmer et al., 2017](#); [Chmiela et al., 2017](#); [Artrith et al., 2017](#); [Unke and Meuwly, 2018](#); [Zhang et al., 2018](#); [Zubatyuk et al., 2019](#); [Smith et al., 2020](#); [Kovács et al., 2021](#)), with increasingly expressive atom environment embeddings and message-passing operations ([Gasteiger et al., 2020b, 2021](#); [Schütt et al., 2021](#); [Liu et al., 2021](#); [Unke et al., 2021a](#); [Chen and Ong, 2022](#); [Deng et al., 2023](#); [Cheng, 2024](#)). Notably, equivariant architectures based on spherical harmonics representations ([Thomas et al., 2018](#); [Thölke and De Fabritiis, 2021](#); [Batzner et al., 2022](#); [Musaelian et al., 2022](#); [Batatia et al., 2022](#); [Passaro and Zitnick, 2023](#); [Liao et al., 2023](#); [Bochkarev et al., 2024](#); [Park et al., 2024](#); [Batatia et al., 2025](#)) have shown strong performance on large-scale datasets. Meanwhile, the



high computational cost of these architectures has sparked significant interest in scalable architectures that may not respect physical principles such as energy conservation (Langer et al., 2024; Brehmer et al., 2024; Hu et al., 2021; Yang et al., 2024; Qu and Krishnapriyan, 2024; Neumann et al., 2024). These models have demonstrated strong performance in accuracy, scalability, and relaxation tasks (Chanussot et al., 2021; Riebesell et al., 2023). While their non-physical nature may make them unsuitable for direct usage in some physical property prediction tasks, they may still provide benefit by using the pre-training strategy proposed in this paper, distilling them to conservative models (Amin et al., 2025), or combining them with a conservative model in a multiple-time-step integration scheme (Bigi et al., 2024).

**MLIPs and physical observables.** While MLIPs continue to improve, it is necessary to evaluate them in realistic tasks that are relevant to scientific discovery. Physical property prediction benchmarks that involve geometry optimization (Riebesell et al., 2023; Lan et al., 2023; Wander et al., 2024), MD simulations (Fu et al., 2023; Kovács et al., 2023; Moore et al., 2024; Sabanes Zariquiey et al., 2024; Eastman et al., 2024), vibrational analysis and phonon calculations (Póta et al., 2024; Loew et al., 2024; Wines and Choudhary, 2024), and others are increasing in scale with broader applications and wider adoption. Training strategies for learning from physical observables (Wang et al., 2020; Greener, 2024; Röcken et al., 2024; Raja et al., 2024) and the higher-order derivatives of the PES (Fang et al., 2024; Williams et al., 2025) are promising directions to further improve MLIPs for predicting physical properties.

## 8 Discussion

We identify conservative forces and a smoothly-varying PES as two important properties for MLIPs to consistently perform well in physical property prediction tasks. We offer an analysis of design choices to enhance these two properties. The resulting eSEN architecture bridges the gap between the test-set error and downstream applications, achieving SOTA performance in force/energy prediction, geometry optimization, phonon calculations, and thermal conductivity prediction. This implies it may be possible to use test error as a proxy metric for evaluating model performance during development, if a model passes energy conservation tests. This can accelerate innovations in MLIPs, since benchmarking physical properties usually requires significant domain knowledge and is usually time-consuming, whereas evaluating test set error is straightforward and efficient.

## Acknowledgements

We acknowledge Zachary W. Ulissi (FAIR at Meta), Aditi S. Krishnapriyan (UC Berkeley), Samuel M. Blau (LBNL) and other members of the FAIR Chemistry team for helpful discussions, and Ammar Rizvi (FAIR at Meta) for project support.

## References

- GJ Ackland, MC Warren, and SJ Clark. Practical methods in ab initio lattice dynamics. *Journal of Physics: Condensed Matter*, 9(37):7861, 1997.
- Ishan Amin, Sanjeev Raja, and Aditi Krishnapriyan. Towards fast, specialized machine learning force fields: Distilling foundation models via energy Hessians. *arXiv preprint arXiv:2501.09009*, 2025.
- Nongnuch Artrith, Alexander Urban, and Gerbrand Ceder. Efficient and accurate machine-learning interpolation of atomic energies in compositions with many species. *Physical Review B*, 96(1):014112, 2017.
- Jimmy Lei Ba. Layer normalization. *arXiv preprint arXiv:1607.06450*, 2016.
- Luis Barroso-Luque, Muhammed Shuaibi, Xiang Fu, Brandon M Wood, Misko Dzamba, Meng Gao, Ammar Rizvi, C Lawrence Zitnick, and Zachary W Ulissi. Open materials 2024 (omat24) inorganic materials dataset and models. *arXiv preprint arXiv:2410.12771*, 2024.
- Christopher J Bartel. Review of computational approaches to predict the thermodynamic stability of inorganic solids. *Journal of Materials Science*, 57(23):10475–10498, 2022.
- Albert P Bartók, Risi Kondor, and Gábor Csányi. On representing chemical environments. *Physical Review B—Condensed Matter and Materials Physics*, 87(18):184115, 2013.
- Ilyes Batatia, David Peter Kovacs, Gregor N. C. Simm, Christoph Ortner, and Gabor Csanyi. MACE: Higher order equivariant message passing neural networks for fast and accurate force fields. In Alice H. Oh, Alekh Agarwal, Danielle Belgrave, and Kyunghyun Cho, editors, *Advances in Neural Information Processing Systems*, 2022. <https://openreview.net/forum?id=YPPpSngE-ZU>.
- Ilyes Batatia, Philipp Benner, Yuan Chiang, Alin M Elena, Dávid P Kovács, Janosh Riebesell, Xavier R Advincula, Mark Asta, Matthew Avaylon, William J Baldwin, et al. A foundation model for atomistic materials chemistry. *arXiv preprint arXiv:2401.00096*, 2023.
- Ilyes Batatia, Simon Batzner, Dávid Péter Kovács, Albert Musaelian, Gregor NC Simm, Ralf Drautz, Christoph Ortner, Boris Kozinsky, and Gábor Csányi. The design space of e (3)-equivariant atom-centred interatomic

- potentials. *Nature Machine Intelligence*, pages 1–12, 2025.
- Simon Batzner, Albert Musaelian, Lixin Sun, Mario Geiger, Jonathan P Mailoa, Mordechai Kornbluth, Nicola Molinari, Tess E Smidt, and Boris Kozinsky. E (3)-equivariant graph neural networks for data-efficient and accurate interatomic potentials. *Nature communications*, 13(1):1–11, 2022.
- Jörg Behler and Michele Parrinello. Generalized neural-network representation of high-dimensional potential-energy surfaces. *Physical review letters*, 98(14):146401, 2007.
- Filippo Bigi, Marcel Langer, and Michele Ceriotti. The dark side of the forces: assessing non-conservative force models for atomistic machine learning. *arXiv preprint arXiv:2412.11569*, 2024.
- Anton Bochkarev, Yury Lysogorskiy, and Ralf Drautz. Graph atomic cluster expansion for semilocal interactions beyond equivariant message passing. *Phys. Rev. X*, 14:021036, Jun 2024. doi: 10.1103/PhysRevX.14.021036. <https://link.aps.org/doi/10.1103/PhysRevX.14.021036>.
- Johann Brehmer, Sönke Behrends, Pim de Haan, and Taco Cohen. Does equivariance matter at scale? *arXiv preprint arXiv:2410.23179*, 2024.
- Lowik Chanussot, Abhishek Das, Siddharth Goyal, Thibaut Lavril, Muhammed Shuaibi, Morgane Riviere, Kevin Tran, Javier Heras-Domingo, Caleb Ho, Weihua Hu, Aini Palizhati, Anuroop Sriram, Brandon Wood, Junwoong Yoon, Devi Parikh, C. Lawrence Zitnick, and Zachary Ulissi. Open catalyst 2020 (oc20) dataset and community challenges. *ACS Catalysis*, 11(10):6059–6072, 2021. doi: 10.1021/acscatal.0c04525. <https://doi.org/10.1021/acscatal.0c04525>.
- Chi Chen and Shyue Ping Ong. A universal graph deep learning interatomic potential for the periodic table. *Nature Computational Science*, 2(11):718–728, 2022.
- Bingqing Cheng. Cartesian atomic cluster expansion for machine learning interatomic potentials. *npj Computational Materials*, 10(1):157, 2024.
- Stefan Chmiela, Alexandre Tkatchenko, Huziel E Sauceda, Igor Poltavsky, Kristof T Schütt, and Klaus-Robert Müller. Machine learning of accurate energy-conserving molecular force fields. *Science advances*, 3(5):e1603015, 2017.
- Stefan Chmiela, Valentin Vassilev-Galindo, Oliver T Unke, Adil Kabylda, Huziel E Sauceda, Alexandre Tkatchenko, and Klaus-Robert Müller. Accurate global machine learning force fields for molecules with hundreds of atoms. *Science Advances*, 9(2):eadf0873, 2023.
- Taco Cohen and Max Welling. Group equivariant convolutional networks. In *International conference on machine learning*, pages 2990–2999. PMLR, 2016.
- Bowen Deng, Peichen Zhong, KyuJung Jun, Janosh Riebesell, Kevin Han, Christopher J Bartel, and Gerbrand Ceder. Chgnet as a pretrained universal neural network potential for charge-informed atomistic modelling. *Nature Machine Intelligence*, 5(9):1031–1041, 2023.
- Peter Eastman, Pavan Kumar Behara, David L Dotson, Raimondas Galvelis, John E Herr, Josh T Horton, Yuezhi Mao, John D Chodera, Benjamin P Pritchard, Yuanqing Wang, et al. Spice, a dataset of drug-like molecules and peptides for training machine learning potentials. *Scientific Data*, 10(1):11, 2023.
- Peter Eastman, Benjamin P Pritchard, John D Chodera, and Thomas E Markland. Nutmeg and spice: models and data for biomolecular machine learning. *Journal of chemical theory and computation*, 20(19):8583–8593, 2024.
- Shiang Fang, Mario Geiger, Joseph G Checkelsky, and Tess Smidt. Phonon predictions with e (3)-equivariant graph neural networks. *arXiv preprint arXiv:2403.11347*, 2024.
- Xiang Fu, Zhenghao Wu, Wujie Wang, Tian Xie, Sinan Keten, Rafael Gomez-Bombarelli, and Tommi S. Jaakkola. Forces are not enough: Benchmark and critical evaluation for machine learning force fields with molecular simulations. *Transactions on Machine Learning Research*, 2023. ISSN 2835-8856. <https://openreview.net/forum?id=A8pqQipwkt>. Survey Certification.
- Brent Fultz. Vibrational thermodynamics of materials. *Progress in Materials Science*, 55(4):247–352, 2010.
- Alex M Ganose, Junsoo Park, Alireza Faghaninia, Rachel Woods-Robinson, Kristin A Persson, and Anubhav Jain. Efficient calculation of carrier scattering rates from first principles. *Nature communications*, 12(1):2222, 2021.
- Johannes Gasteiger, Janek Groß, and Stephan Günnemann. Directional message passing for molecular graphs. *arXiv preprint arXiv:2003.03123*, 2020a.
- Johannes Gasteiger, Janek Groß, and Stephan Günnemann. Directional message passing for molecular graphs. In *International Conference on Learning Representations*, 2020b.
- Johannes Gasteiger, Florian Becker, and Stephan Günnemann. Gemnet: Universal directional graph neural networks for molecules. *Advances in Neural Information Processing Systems*, 34:6790–6802, 2021.
- Mario Geiger and Tess Smidt. e3nn: Euclidean neural networks. *arXiv preprint arXiv:2207.09453*, 2022.
- Justin Gilmer, Samuel S Schoenholz, Patrick F Riley, Oriol Vinyals, and George E Dahl. Neural message passing for quantum chemistry. In *International conference on machine learning*, pages 1263–1272. PMLR, 2017.

- Joe G Greener. Differentiable simulation to develop molecular dynamics force fields for disordered proteins. *Chemical Science*, 15(13):4897–4909, 2024.
- Ernst Hairer, Christian Lubich, and Gerhard Wanner. Geometric numerical integration illustrated by the störmer–verlet method. *Acta numerica*, 12:399–450, 2003.
- Ernst Hairer, Marlis Hochbruck, Arieh Iserles, and Christian Lubich. Geometric numerical integration. *Oberwolfach Reports*, 3(1):805–882, 2006.
- Weihua Hu, Muhammed Shuaibi, Abhishek Das, Sidharth Goyal, Anuroop Sriram, Jure Leskovec, Devi Parikh, and C Lawrence Zitnick. Forcenet: A graph neural network for large-scale quantum calculations. *arXiv preprint arXiv:2103.01436*, 2021.
- A Jain, SP Ong, G Hautier, W Chen, WD Richards, S Dacek, S Cholia, D Gunter, D Skinner, G Ceder, et al. The materials project: a materials genome approach to accelerating materials innovation. *apl mater* 1: 011002, 2013.
- Dávid Péter Kovács, Cas van der Oord, Jiri Kucera, Alice EA Allen, Daniel J Cole, Christoph Ortner, and Gábor Csányi. Linear atomic cluster expansion force fields for organic molecules: beyond rmse. *Journal of chemical theory and computation*, 17(12):7696–7711, 2021.
- Dávid Péter Kovács, J Harry Moore, Nicholas J Brown-ing, Ilyes Batatia, Joshua T Horton, Venkat Kapil, William C Witt, Ioan-Bogdan Magdău, Daniel J Cole, and Gábor Csányi. Mace-off23: Transferable machine learning force fields for organic molecules. *arXiv preprint arXiv:2312.15211*, 2023.
- Janice Lan, Aini Palizhati, Muhammed Shuaibi, Brandon M Wood, Brook Wander, Abhishek Das, Matt Uytendaele, C Lawrence Zitnick, and Zachary W Ulissi. Adsorbml: a leap in efficiency for adsorption energy calculations using generalizable machine learning potentials. *npj Computational Materials*, 9(1):172, 2023.
- Marcel F Langer, Sergey N Pozdnyakov, and Michele Ceriotti. Probing the effects of broken symmetries in machine learning. *Machine Learning: Science and Technology*, 5(4):04LT01, 2024.
- Ask Hjorth Larsen, Jens Jørgen Mortensen, Jakob Blomqvist, Ivano E Castelli, Rune Christensen, Marcin Dułak, Jesper Friis, Michael N Groves, Bjørk Hammer, Cory Hargus, Eric D Hermes, Paul C Jennings, Peter Bjerre Jensen, James Kermode, John R Kitchin, Esben Leonhard Kolsbjerg, Joseph Kubal, Kristen Kaasbjerg, Steen Lysgaard, Jón Bergmann Maronsson, Tristan Maxson, Thomas Olsen, Lars Pastewka, Andrew Peterson, Carsten Rostgaard, Jakob Schiøtz, Ole Schütt, Mikkel Strange, Kristian S Thygesen, Tejs Vegge, Lasse Vilhelmsen, Michael Walter, Zhenhua Zeng, and Karsten W Jacobsen. The atomic simulation environment—a python library for working with atoms. *Journal of Physics: Condensed Matter*, 29(27):273002, 2017. <http://stacks.iop.org/0953-8984/29/i=27/a=273002>.
- Yi-Lun Liao and Tess Smidt. Equiformer: Equivariant graph attention transformer for 3d atomistic graphs. *arXiv preprint arXiv:2206.11990*, 2022.
- Yi-Lun Liao, Brandon Wood, Abhishek Das, and Tess Smidt. Equiformerv2: Improved equivariant transformer for scaling to higher-degree representations. *arXiv preprint arXiv:2306.12059*, 2023.
- Yi-Lun Liao, Tess Smidt, and Abhishek Das. Generalizing denoising to non-equilibrium structures improves equivariant force fields. *arXiv preprint arXiv:2403.09549*, 2024.
- Yi Liu, Limei Wang, Meng Liu, Yuchao Lin, Xuan Zhang, Bora Oztekin, and Shuiwang Ji. Spherical message passing for 3d molecular graphs. In *International Conference on Learning Representations*, 2021.
- Antoine Loew, Dewen Sun, Hai-Chen Wang, Silvana Botti, and Miguel AL Marques. Universal machine learning interatomic potentials are ready for phonons. *arXiv preprint arXiv:2412.16551*, 2024.
- Amil Merchant, Simon Batzner, Samuel S Schoenholz, Muratahan Aykol, Gwoon Cheon, and Ekin Dogus Cubuk. Scaling deep learning for materials discovery. *Nature*, 624(7990):80–85, 2023.
- J Harry Moore, Daniel J Cole, and Gabor Csanyi. Computing hydration free energies of small molecules with first principles accuracy. *arXiv preprint arXiv:2405.18171*, 2024.
- Albert Musaelian, Simon Batzner, Anders Johansson, Lixin Sun, Cameron J Owen, Mordechai Kornbluth, and Boris Kozinsky. Learning local equivariant representations for large-scale atomistic dynamics. *arXiv preprint arXiv:2204.05249*, 2022.
- Mark Neumann, James Gin, Benjamin Rhodes, Steven Bennett, Zhiyi Li, Hitarth Choubisa, Arthur Hussey, and Jonathan Godwin. Orb: A fast, scalable neural network potential. *arXiv preprint arXiv:2410.22570*, 2024.
- John Nickolls, Ian Buck, Michael Garland, and Kevin Skadron. Scalable parallel programming with cuda: Is cuda the parallel programming model that application developers have been waiting for? *Queue*, 6(2):40–53, 2008.
- MBJR Oppenheimer. Zur quantentheorie der molekeln [on the quantum theory of molecules]. *Annalen der Physik*, 389(20):457–484, 1927.
- Cameron J Owen, Steven B Torrisi, Yu Xie, Simon Batzner, Kyle Bystrom, Jennifer Coulter, Albert Musaelian, Lixin Sun, and Boris Kozinsky. Complexity of many-body interactions in transition metals via

- machine-learned force fields from the tm23 data set. *npj Computational Materials*, 10(1):92, 2024.
- Yutack Park, Jaesun Kim, Seungwoo Hwang, and Seungwu Han. Scalable parallel algorithm for graph neural network interatomic potentials in molecular dynamics simulations. *J. Chem. Theory Comput.*, 20(11):4857–4868, 2024. doi: 10.1021/acs.jctc.4c00190.
- Robert G Parr, Shridhar R Gadre, and Libero J Bartolotti. Local density functional theory of atoms and molecules. *Proceedings of the National Academy of Sciences*, 76(6):2522–2526, 1979.
- Saro Passaro and C Lawrence Zitnick. Reducing so (3) convolutions to so (2) for efficient equivariant gnns. In *International Conference on Machine Learning*, pages 27420–27438. Proceedings of Machine Learning Research, 2023.
- Adam Paszke, Sam Gross, Francisco Massa, Adam Lerer, James Bradbury, Gregory Chanan, Trevor Killeen, Zeming Lin, Natalia Gimelshein, Luca Antiga, et al. Pytorch: An imperative style, high-performance deep learning library. *Advances in neural information processing systems*, 32, 2019.
- Balázs Póta, Paramvir Ahlawat, Gábor Csányi, and Michele Simoncelli. Thermal conductivity predictions with foundation atomistic models. *arXiv preprint arXiv:2408.00755*, 2024.
- Eric Qu and Aditi S. Krishnapriyan. The importance of being scalable: Improving the speed and accuracy of neural network interatomic potentials across chemical domains. In *The Thirty-eighth Annual Conference on Neural Information Processing Systems*, 2024. <https://openreview.net/forum?id=Y4mBaZu4vy>.
- Sanjeev Raja, Ishan Amin, Fabian Pedregosa, and Aditi S Krishnapriyan. Stability-aware training of neural network interatomic potentials with differentiable boltzmann estimators. *arXiv preprint arXiv:2402.13984*, 2024.
- Manijeh Razeghi. Thermal Properties of Crystals. In Manijeh Razeghi, editor, *Fundamentals of Solid State Engineering*, pages 197–220. Springer US, 2002. doi: 10.1007/0-306-47567-7\_7.
- Janosh Riebesell, Rhys EA Goodall, Anubhav Jain, Philipp Benner, Kristin A Persson, and Alpha A Lee. Matbench discovery—an evaluation framework for machine learning crystal stability prediction. *arXiv preprint arXiv:2308.14920*, 2023.
- Sebastien Röcken, Anton F Burnet, and Julija Zavadlav. Predicting solvation free energies with an implicit solvent machine learning potential. *arXiv preprint arXiv:2406.00183*, 2024.
- Francesc Sabanes Zariquiey, Raimondas Galvelis, Emilio Gallicchio, John D Chodera, Thomas E Markland, and Gianni De Fabritiis. Enhancing protein–ligand binding affinity predictions using neural network potentials. *Journal of Chemical Information and Modeling*, 64(5):1481–1485, 2024.
- Jonathan Schmidt, Tiago FT Cerqueira, Aldo H Romero, Antoine Loew, Fabian Jäger, Hai-Chen Wang, Silvana Botti, and Miguel AL Marques. Improving machine-learning models in materials science through large datasets. *Materials Today Physics*, 48:101560, 2024.
- Kristof Schütt, Pieter-Jan Kindermans, Huziel Enoc Saucedo Felix, Stefan Chmiela, Alexandre Tkatchenko, and Klaus-Robert Müller. Schnet: A continuous-filter convolutional neural network for modeling quantum interactions. *Advances in neural information processing systems*, 30, 2017.
- Kristof Schütt, Oliver Unke, and Michael Gastegger. Equivariant message passing for the prediction of tensorial properties and molecular spectra. In *International Conference on Machine Learning*, pages 9377–9388. PMLR, 2021.
- Michele Simoncelli, Nicola Marzari, and Francesco Mauri. Wigner formulation of thermal transport in solids. *Physical Review X*, 12(4):041011, 2022.
- Justin S Smith, Olexandr Isayev, and Adrian E Roitberg. Ani-1: an extensible neural network potential with dft accuracy at force field computational cost. *Chemical science*, 8(4):3192–3203, 2017.
- Justin S Smith, Roman Zubatyuk, Benjamin Nebgen, Nicholas Lubbers, Kipton Barros, Adrian E Roitberg, Olexandr Isayev, and Sergei Tretiak. The ani-1ccx and ani-1x data sets, coupled-cluster and density functional theory properties for molecules. *Scientific data*, 7(1):134, 2020.
- Philipp Thölke and Gianni De Fabritiis. Equivariant transformers for neural network based molecular potentials. In *International Conference on Learning Representations*, 2021.
- Nathaniel Thomas, Tess Smidt, Steven Kearnes, Lusann Yang, Li Li, Kai Kohlhoff, and Patrick Riley. Tensor field networks: Rotation-and translation-equivariant neural networks for 3d point clouds. *arXiv preprint arXiv:1802.08219*, 2018.
- Atsushi Togo, Laurent Chaput, and Isao Tanaka. Distributions of phonon lifetimes in brillouin zones. *Phys. Rev. B*, 91:094306, Mar 2015. doi: 10.1103/PhysRevB.91.094306.
- Atsushi Togo, Laurent Chaput, Terumasa Tadano, and Isao Tanaka. Implementation strategies in phonopy and phono3py. *J. Phys. Condens. Matter*, 35(35):353001, 2023. doi: 10.1088/1361-648X/acd831.
- Richard Tran, Janice Lan, Muhammed Shuaibi, Brandon M Wood, Siddharth Goyal, Abhishek Das, Javier Heras-Domingo, Adeesh Kolluru, Ammar Rizvi, Nima Shoghi, et al. The open catalyst 2022 (oc22) dataset and challenges for oxide electrocatalysts. *ACS Catalysis*, 13(5):3066–3084, 2023.

- Mark E Tuckerman. *Statistical mechanics: theory and molecular simulation*. Oxford university press, 2023.
- Oliver T Unke and Markus Meuwly. A reactive, scalable, and transferable model for molecular energies from a neural network approach based on local information. *The Journal of chemical physics*, 148(24):241708, 2018.
- Oliver T Unke, Stefan Chmiela, Michael Gastegger, Kristof T Schütt, Huziel E Sauceda, and Klaus-Robert Müller. SpookyNet: Learning force fields with electronic degrees of freedom and nonlocal effects. *Nature communications*, 12(1):1–14, 2021a.
- Oliver T Unke, Stefan Chmiela, Huziel E Sauceda, Michael Gastegger, Igor Poltavsky, Kristof T Schütt, Alexandre Tkatchenko, and Klaus-Robert Müller. Machine learning force fields. *Chemical Reviews*, 121(16):10142–10186, 2021b.
- Axel Van De Walle and Gerbrand Ceder. The effect of lattice vibrations on substitutional alloy thermodynamics. *Reviews of Modern Physics*, 74(1):11, 2002.
- Brook Wander, Muhammed Shuaibi, John R Kitchin, Zachary W Ulissi, and C Lawrence Zitnick. Cattsunami: Accelerating transition state energy calculations with pre-trained graph neural networks. *arXiv preprint arXiv:2405.02078*, 2024.
- Wujie Wang, Simon Axelrod, and Rafael Gómez-Bombarelli. Differentiable molecular simulations for control and learning. *arXiv preprint arXiv:2003.00868*, 2020.
- Maurice Weiler, Mario Geiger, Max Welling, Wouter Boomsma, and Taco S Cohen. 3d steerable cnns: Learning rotationally equivariant features in volumetric data. *Advances in Neural Information Processing Systems*, 31, 2018.
- Nicholas J Williams, Lara Kabalan, Ljiljana Stojanovic, Viktor Zólyomi, and Edward O Pyzer-Knapp. Hessian qm9: A quantum chemistry database of molecular Hessians in implicit solvents. *Scientific Data*, 12(1):9, 2025.
- Daniel Wines and Kamal Choudhary. Chips-ff: Evaluating universal machine learning force fields for material properties. *arXiv preprint arXiv:2412.10516*, 2024.
- Han Yang, Chenxi Hu, Yichi Zhou, Xixian Liu, Yu Shi, Jielan Li, Guanzhi Li, Zekun Chen, Shuizhou Chen, Claudio Zeni, et al. Mattersim: A deep learning atomistic model across elements, temperatures and pressures. *arXiv preprint arXiv:2405.04967*, 2024.
- Linfeng Zhang, Jiequn Han, Han Wang, Wissam Saidi, Roberto Car, et al. End-to-end symmetry preserving inter-atomic potential energy model for finite and extended systems. *Advances in Neural Information Processing Systems*, 31, 2018.
- Larry Zitnick, Abhishek Das, Adeesh Kolluru, Janice Lan, Muhammed Shuaibi, Anuroop Sriram, Zachary Ulissi, and Brandon Wood. Spherical channels for modeling atomic interactions. *Advances in Neural Information Processing Systems*, 35:8054–8067, 2022.
- Roman Zubatyuk, Justin S Smith, Jerzy Leszczynski, and Olexandr Isayev. Accurate and transferable multi-task prediction of chemical properties with an atom-in-molecules neural network. *Science advances*, 5(8):eaav6490, 2019.

## A Experimental details

### A.1 MD simulation protocol

Simulating molecular systems not seen during training is a key capability of MLIPs. Therefore, we construct challenging MD simulation tasks featuring out-of-distribution data to test a model’s conservation capability. We conduct experiments on two chemical domains: inorganic crystals and organic molecules.

**Inorganic materials.** For training models on inorganic materials we utilize the MPTrj (Deng et al., 2023) dataset, and we establish a suite of simulation tasks based on the TM23 dataset (Owen et al., 2024). TM23 contains MD samples of 27 single vacancy defect transition metal systems at cold, warm, and melt temperatures using an NVT ensemble, in total 81 combinations of different metals and temperature. These defected systems are out-of-distribution for a model trained on the MPTrj datasets, which only contains relaxation trajectories of non-defected systems. Additionally, some of the metals in the TM23 dataset is very rare in the MPTrj dataset. We initialize the simulation by sampling a frame from the TM23 dataset, run a relaxation using the LBFGS algorithm, randomly initialize the atom velocities at cold/warm/melt temperatures using a Maxwell-Boltzmann distribution, then run MD simulations under the NVE ensemble for 100 ps using a time step of 5 fs (same as the time step used in the TM23 ab initio MD protocol).

**Organic molecules.** For training models on organic molecules we use the SPICE-MACE-OFF dataset (Kovács et al., 2023), which is mainly based on the SPICE-1.0 dataset (Eastman et al., 2023), and we establish a suite of simulation tasks from the MD22 dataset (Chmiela et al., 2023) that contains seven large molecules. Molecules in MD22 are out-of-distribution for a model trained on the SPICE-MACE-OFF dataset as they are considerably larger than all molecules in the SPICE-MACE-OFF training dataset. We initialize the simulation by sampling a frame from the MD22 dataset, run a relaxation using the LBFGS algorithm, randomly initialize the atom velocities at a temperatures of 400/500 K using a Maxwell-Boltzmann distribution (400 K for Buckyball catcher and Double-walled nanotube and 500 K for other molecules, which are the same as the MD22 protocol), then run MD simulations under the NVE ensemble for 100 ps using a time step of 1 fs (same as the time step used in the MD22 ab initio MD protocol).

All ML-based MD simulations use a Velocity-Verlet

integrator and are conducted with ASE (Larsen et al., 2017). We measure the energy conservation error (extent of energy drift) across the 100-ps simulations. All eSEN models are 2-layer with  $L_{\max} = 2$  and  $M_{\max} = 2$  (3.2M trainable parameters). Detailed model hyperparameters are included in Appendix D.

### A.2 Phonon calculation protocols

Harmonic and anharmonic phonon calculations and solutions to the Wigner transport equation (Simoncelli et al., 2022) used for the thermal conductivity benchmark ( $\kappa_{\text{SRME}}$ ) values given in Table 2 were carried out using the supercell method with finite differences implemented in PHONO3PY (Togo et al., 2015, 2023). The calculations followed the protocol described in the Matbench-Discovery benchmark (Riebesell et al., 2023; Póta et al., 2024). For eSEN-30M, an even lower  $\kappa_{\text{SRME}}$  of 0.298 is obtained when we adjust the evaluation parameter atom displacement from 0.03 Å to 0.05 Å.

Harmonic phonon calculations for the MDR benchmark results listed in Section 6.2 were carried out following the calculation protocol used by (Loew et al., 2024) which employs phonon calculations using the supercell method with finite differences with a displacement of 0.01 Å. Calculations were done using the PHONOPY software Togo et al. (2023).

### A.3 Test-set error for MPTrj-trained models

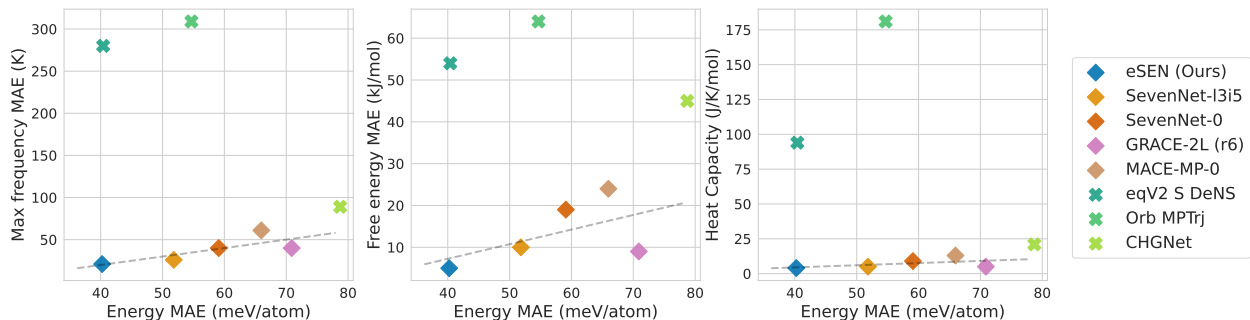
Since MPTrj lacks an official test split and various models are typically trained on distinct subsets of the data, we randomly selected 5000 samples from the subsampled Alexandria (sAlex) dataset (Schmidt et al., 2024; Barroso-Luque et al., 2024) for a fair comparison. This subset was used to calculate the test-set energy mean absolute errors (MAEs) presented in Figures 1, 6, B.7, and B.8.

## B Phonon calculations

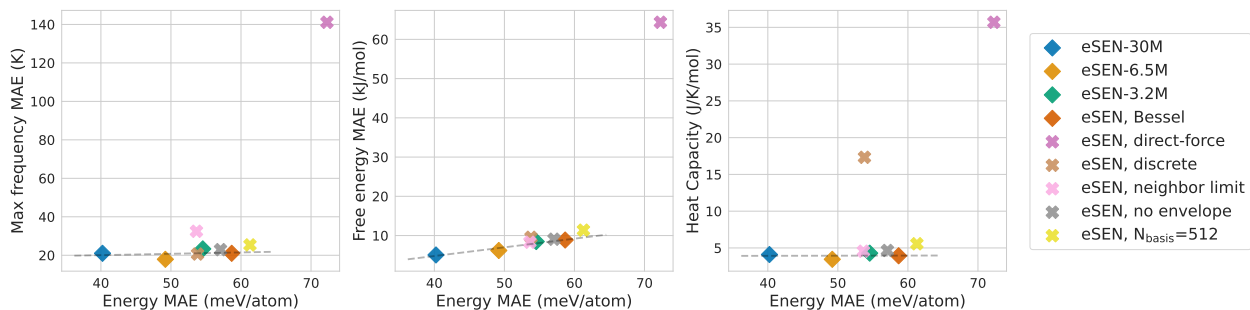
### B.1 Correlation of test-set energy errors and vibrational property errors

Figure B.7 presents the correlation between test-set energy MAE and the other three phonon calculation tasks, evaluated across various model architectures. The corresponding correlations for different variants of eSEN are displayed in Figure B.8. In both figures, improved correlation can be observed among energy-conserving models.

Figure B.8 illustrates that failing the conservation



**Figure B.7** The correlation between test-set energy error and maximum frequency, free energy and heat capacity across different model architectures.



**Figure B.8** The correlation between test-set energy error and maximum frequency, free energy and heat capacity for different variants of eSEN.

test can result in varying degrees of impact on different properties, depending on the specific design choices made. Although the neighbor limit, envelope function, and number of basis functions substantially affect  $\kappa_{\text{SRME}}$  (see Figure 6), their influence on the properties evaluated in the MDR Phonon benchmark is relatively minor. Representation discretization impacts vibrational entropy and heat capacity but not other properties. While a model might still be able to get good performance in some physical property task when the energy conservation test is failed, when the conservation test is passed, the model performs very well robustly across all metrics.

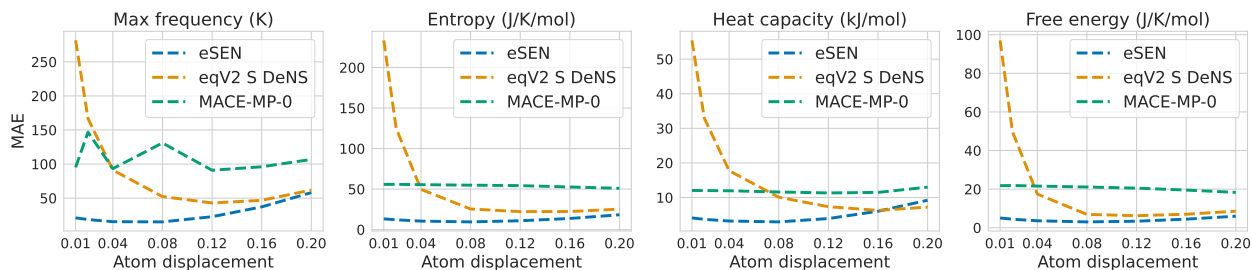
## B.2 Displacement values and their relation to phonon band structure predictions

Figure B.9 presents the MAEs on phonon calculations for eSEN, MACE, and eqV2 S DeNS as a function of increasing displacement values. As anticipated, both eSEN and MACE exhibit constant or slightly increasing MAE with respect to displacement. In contrast, eqV2 S DeNS displays a notable decrease in MAE with increasing displacement. Notably, when using a displacement of 0.2 Å, the resulting phonon benchmark MAE values for eqV2 S DeNS become comparable to those of conservative force models

(Section 6.2).

While the prediction accuracy of thermodynamic properties such as maximum frequency, entropy, free energy, and heat capacity improves with increasing displacement for direct-force models, this improvement is deceptive and does not translate to accurate predictions of the underlying phonon band structure and density of states (DOS). As illustrated in Figure C.11, the predicted phonon bands and DOS for three selected materials exhibit significant errors, particularly in capturing the correct dispersion relations. Moreover, imaginary frequencies are commonly predicted at small displacement values, suggesting a rough energy landscape (i.e. the learned PES is not truly convex when it’s very close to the minima). The eqV2 S DeNS model also fails to accurately capture acoustic modes—those that go to zero linearly at the  $\gamma$  point—which is due to a non-zero net force on the structure. In contrast, non-zero net force at energy local minima does not occur for conservative models by definition (Figure 5).

By enforcing a net zero force prediction, as proposed by Neumann et al. 2024, direct-force models can be modified to accurately capture acoustic phonon modes. As demonstrated in Figure C.12, incorporating this constraint allows the model to predict



**Figure B.9** Errors in a randomly sampled subset (1000 samples) of the MDR Phonon benchmark when the atom displacement is adjusted.

acoustic modes correctly. However, despite this improvement, the model continues to struggle with accurately reproducing the phonon band structure, and the issue of predicting imaginary frequencies at small displacement values persists.

The apparent paradox of direct-force models like eqV2 S DeNS failing to accurately capture phonon band structures while still achieving competitive accuracy for thermodynamic properties such as entropy, free energy, and heat capacity can be resolved by examining the underlying calculation methodology. These properties are computed using weighted integrals of the DOS. Additionally the metrics in the MDR are performed at room temperature (300 K). The predicted DOS in Figure C.11 and Figure C.12 at larger displacement values adequately captures the overall features of the DFT DOS, but does not reproduce finer details such as high density areas and fluctuations. This level of agreement is sufficient for accurate predictions because the Boltzmann-weighted integrals used in calculating thermal properties help to mitigate the impact of point-wise errors, making it less crucial to precisely capture fine details in the band structure and DOS Ackland et al. (1997); Van De Walle and Ceder (2002). Moreover, since properties are estimated at 300 K, models can achieve accurate predictions by prioritizing prediction accuracy of lower-frequency modes, which are more relevant for thermal property calculations, rather than attempting to capture higher-frequency modes. Although eqV2 S DeNS without a net-zero force constraint may not accurately capture acoustic phonon branches, its ability to predict vibrational thermodynamics at room temperature remains unaffected due to the relatively small number of acoustic phonon states at low frequencies.

As a comparison with eqV2 S DeNS, Figures Figure C.13 and Figure C.14 shows the predicted phonon dispersion and DOS for the same materials using eSEN with direct-force prediction. Although the results still exhibit some of the characteristic artifacts

of direct-force models, such as convergence at larger displacements and the absence of acoustic modes, these issues are less pronounced compared to eqV2 S DeNS. Moreover, the predicted phonon bands and DOS are significantly improved, providing a more accurate representation of the DFT reference values. The better approximation of phonon bands and a lower tendency to predict imaginary frequencies highlight the importance of a smoothly-varying model, even without being conservative.

Extending the existing metrics proposed by Loew et al. 2024 with additional evaluations would provide a more comprehensive assessment of MLIP performance. Specifically, new metrics could be developed to assess phonon dispersion across all modes and frequencies at commensurate points; and computing vibrational thermodynamic properties at a range of temperatures.

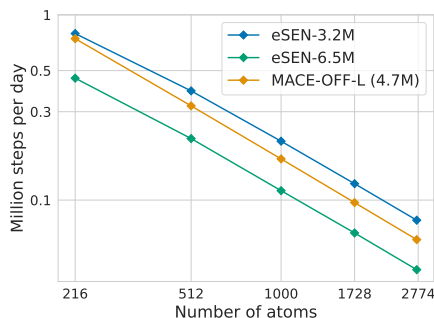


**Figure B.10** Inference efficiency of MACE-OFF-L and eSENs of a similar scale.

## C Inference efficiency

We benchmarked the inference speed of our models against the similar sized MACE-OFF-L (Kovács et al., 2023) (4.7M) on a single 80GB Nvidia A-100 GPU. For MACE-OFF-L we used the exact benchmark code found in [https://github.com/ACEsuit/mace/blob/main/tests/test\\_benchmark.py](https://github.com/ACEsuit/mace/blob/main/tests/test_benchmark.py) with mace-torch



v0.3.6 (PyPi). To create a fair comparison, we replicated the identical benchmark environment as MACE benchmarks using the same diamond system with variable number of supercells (carbon atoms) as input. All models are benchmarked using the standard Python (3.12) runtime with Pytorch v2.4.0 (Paszke et al., 2019) and CUDA 12.1 (Nickolls et al., 2008). No compile/torchscript was used for standardization of runtime. Across all system sizes, eSEN-3.2M has a comparable inference efficiency to MACE-OFF-L. For 216 atoms (Figure B.10), our models (3.2M, 6.4M) can run approximately (0.4, 0.8) million steps per day comparable to MACE-OFF-L (0.7 million steps per day).

## D Hyper-parameters

Hyper-parameters used for model training are shown in Table 5. We train all models using a per-atom energy MAE loss, a force  $l_2$  loss, and a stress MAE loss. For direct-force models or direct-force pre-training, we use the same decomposed loss as described in Barroso-Luque et al. 2024. The eSEN-30M model trained on MPTrj uses Denoising Non-equilibrium Structures (DeNS) (Liao et al., 2024) with a noising probability of 0.5, a standard deviation of 0.1 Å for the added Gaussian noise, and 10 for the DeNS loss coefficient during direct-force pre-training. DeNS is not used during conservative fine-tuning. In our ablation study for maximum neighbor limit we used 30 as the limit.

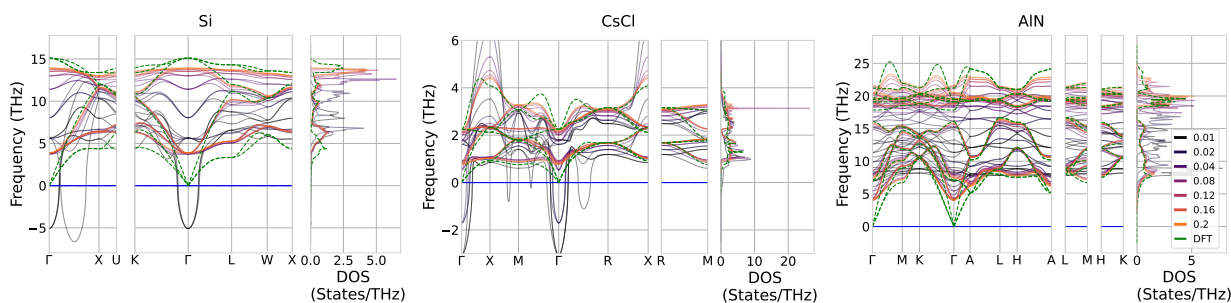


**Figure C.11** Predicted phonon band structure and density of states (DOS) of Si (diamond structure), CsCl (CsCl structure), AlN (wurtzite structure) using eqV2 S DeNS (direct-force prediction) at different displacement values. DFT baseline is taken from the PBE MDR dataset [Loew et al. \(2024\)](#) calculated using a displacement of 0.01 Å

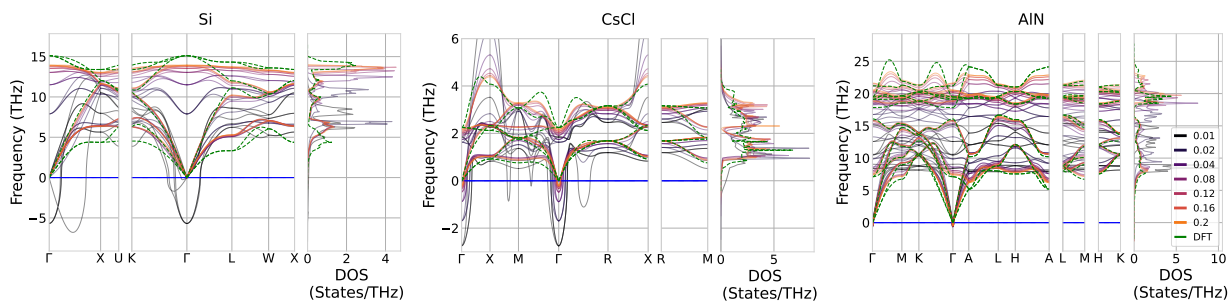


**Figure C.12** Predicted phonon band structure and density of states (DOS) of Si (diamond structure), CsCl (CsCl structure), AlN (wurtzite structure) using eqV2 S DeNS (direct-force prediction with a zero net force constraint) at different displacement values. DFT baseline is taken from the PBE MDR dataset [Loew et al. \(2024\)](#) calculated using a displacement of 0.01 Å

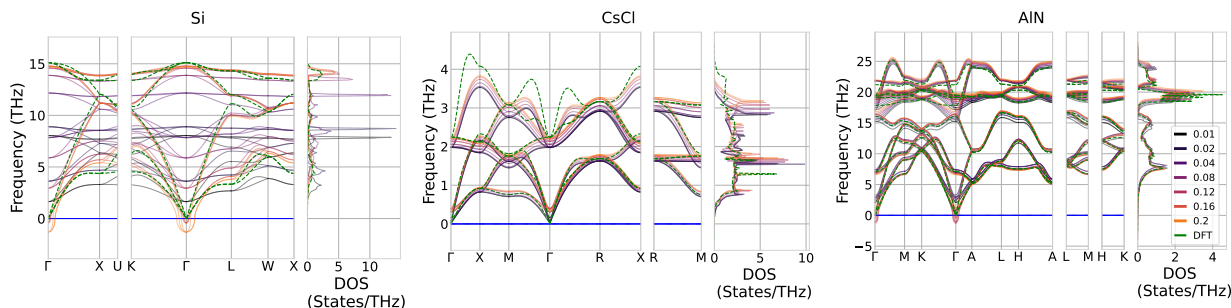


**Figure C.13** Predicted phonon band structure and density of states (DOS) of Si (diamond structure), CsCl (CsCl structure), AlN (wurtzite structure) using eSEN with direct-force prediction at different displacement values. DFT baseline is taken from the PBE MDR dataset [Loew et al. \(2024\)](#) calculated using a displacement of 0.01 Å

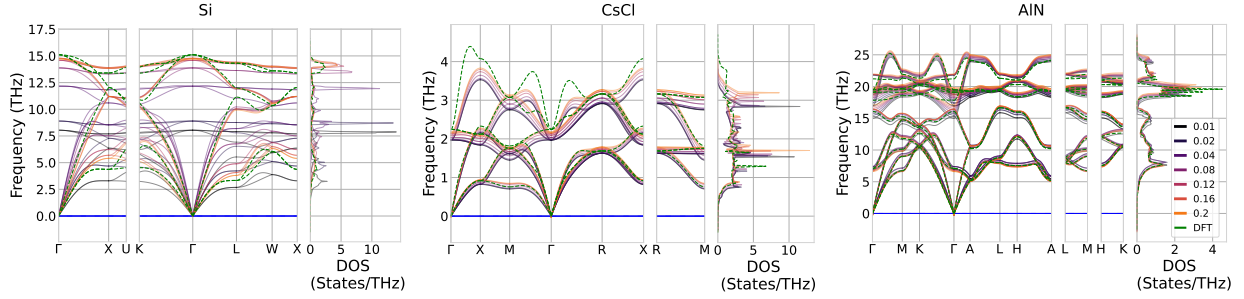


**Figure C.14** Predicted phonon band structure and density of states (DOS) of Si (diamond structure), CsCl (CsCl structure), AlN (wurtzite structure) using eSEN with direct-force prediction and a zero-net force constraint at different displacement values. DFT baseline is taken from the PBE MDR dataset [Loew et al. \(2024\)](#) calculated using a displacement of 0.01 Å

**Table 5** Hyper-parameters for eSEN trained on MPTrj/SPICE-MACE-OFF. \* eSEN-30M on MPTrj was trained for 60 epochs using direct-force pre-training and 40 epochs of conserved fine-tuning.

Hyper-parameters	SPICE-3.2M	SPICE-6.5M	MPTrj-3.2M	MPTrj-6.5M	MPTrj-30M
Number of eSEN layer blocks	2	4	2	4	10
Maximum degree $L_{\max}$	2	2	2	2	3
Maximum order $M_{\max}$	2	2	2	2	2
Number of channels $N_{\text{channel}}$	128	128	128	128	128
Radial basis function	Bessel	Bessel	Gaussian	Gaussian	Gaussian
Number of radial basis functions	10	10	10	10	10
Cutoff radius (Å)	5	5	6	6	6
Batch size	128	128	512	512	512
Optimizer	AdamW	AdamW	AdamW	AdamW	AdamW
Learning rate scheduling	Cosine	Cosine	Cosine	Cosine	Cosine
Warmup epochs	0.1	0.01	0.1	0.1	0.1
Warmup factor	0.2	0.2	0.2	0.2	0.2
Maximum learning rate	$4 \times 10^{-4}$	$4 \times 10^{-4}$	$4 \times 10^{-4}$	$4 \times 10^{-4}$	$4 \times 10^{-4}$
Number of epochs	100	100	100	100	60 + 40*
Gradient clipping norm threshold	100	100	100	100	100
Model EMA decay	0.999	0.999	0.999	0.999	0.999
Weight decay	$1 \times 10^{-3}$	$1 \times 10^{-3}$	$1 \times 10^{-3}$	$1 \times 10^{-3}$	$1 \times 10^{-3}$
Energy loss coefficient	10	10	1	1	20
Force loss coefficient	20	20	10	10	20
Stress loss coefficient	-	-	100	100	5